SPECTRAL, STRUCTURAL, STABILITY CHARACTERISTICS AND FRONTIER MOLECULAR ORBITALS OF TRI-N-BUTYL PHOSPHATE (TBP) AND ITS DEGRADATION PRODUCTS: DFT CALCULATIONS

R. K. HUSSEIN[a], H. M. ELKHAIR[b,c], A. O. ELZUPIR[b,*], K. H. IBNAOUF[a,]
[a]*Imam Mohammad Ibn Saud Islamic University (IMSIU), College of Science, Physics department P.O.Box 90950, Riyadh 11623, Saudi Arabia*
[b]*Imam Mohammad Ibn Saud Islamic University (IMSIU), College of Science, Deanship of Scientific Research, Riyadh, Saudi Arabia*
[c] *Department of Physics, Al Neelain University, P. O. Box 12702, Khartoum 11121, Sudan.*

This work demonstrates the facilities offered by density functional theory (DFT) to calculate the molecular structural and spectral properties of tri-n-butyl phosphate (TBP) and its derivatives, namely, di-n-butyl phosphate (HDBP) and mono-n-butyl phosphate (H_2MBP). The computed parameters including frontier molecular orbitals and HOMO-LUMO transitions indicated the TBP has the lowermost total energy with a lager HOMO-LUMO energy bandgap followed by HDBP and H2MBP. These outcomes in terms of reactivity and stability were reversed counting their dipole moments. The simulated spectra of FTIR and Raman suggested these techniques could be considered as powerful for qualitative analysis of these compounds.

(Received September 10, 2020; Accepted January 13, 2021)

Keywords: Rri-n-butyl phosphate (TBP), Density functional theory, HOMO-LUMO transitions, Frontier molecular orbitals, Energy band gap, Stability

1. Introduction

Tributyl phosphate (TBP) one of the most important chemicals utilized in various industrial applications including as plasticizers, as a binder for paints and pigments, as de-foamers, as a primary component in hydraulic fluids, fire retardants and in agriculture as herbicides. In addition, the TBP can be used as an organic solvent to extract minerals from rocks [1–4]. The most important use of TBP is in extracting the hexavalent uranium and the tetravalent plutonium, to form radioactive complexes in the processing of nuclear fuel by the PUREX process (Plutonium Uranium Refining by Extraction) [5–9]. Thus, it is not surprising that TBP and its derivatives have recently been documented as newly emerging pollutants of the environments and, therefore, may pose health hazards for humans and animals [10–12]. The TBP has been detected even in indoor dust. [13, 14].

The TBP is found to degrade to di-n-butyl phosphate (HDBP) and mono-n-butyl phosphate (H2MBP). This process includes the replacement of one or two n-butyl groups by proton and takes place during the radiolysis reactions using 30% TBP in alkane diluent and 1 M–3 M aqueous nitric acid [15–18]. The lack of information concerning chemical and physical properties of TBP and its derivatives have strongly motivated a number of researchers to carry out theoretical and experimental work [19–23].

In this study, the molecular, structural and spectral properties of tri-n-butyl phosphate (TBP) and its derivatives HDBP and H2MBP have been thoroughly studied. The energy gap, HOMO-LUMO transitions, frontier molecular orbitals, dipole moment, and electron charges distribution, Raman and infrared spectra were obtained using the DFT package. The

* Corresponding author: aminosman81@gmail.com

2. Computational method

The optimized energy structures for TBP, HDBP, and HMBP were calculated using DFT, HOMO-LUMO transitions, frontier molecular orbitals, FTIR spectra, Raman spectra. Dipole moment and electron charge distribution were estimated by the B3LYP method alongside 6-31G** basis sets. ORCA version 4.0.0 program (modern electronic structure package) has been used for calculating the parameters [24-27]. Avogadro software was used for visualizing Mulliken charge, static electro-potential, and frontier molecular orbitals [28], whereas the FT-IR and Raman data were plotted by Gabedit packages [29].

3. Results and discussions

3.1. Energy and HOMO-LUMO Interactions

The optimized structures of TBP, HDBP, and H_2MBP are shown in Fig.1. The HOMO is primarily located within phosphine, oxygen and CH_2 group immediately next to oxygen atoms as expected. The LUMO is composed of a sizeable antibonding orbital with slightly less out of phase interactions for each molecule as shown in Fig. 2. The total energy and energy gap (the difference between HOMO and LUMO molecular orbital) are an important descriptor for the stability and reactivity. The total energy, the HOMO and LUMO energies and the HOMO-LUMO bandgap (ΔE_g) are shown in Table 1. The HOMO-LUMO transitions exhibited the energy gap of TBP is greater than the energy band gaps of HDBP and H_2MBP. These results suggest that the stability of TBP is higher than that of its derivatives, but another factor is involved and reverse this observation, it is dipole moment.

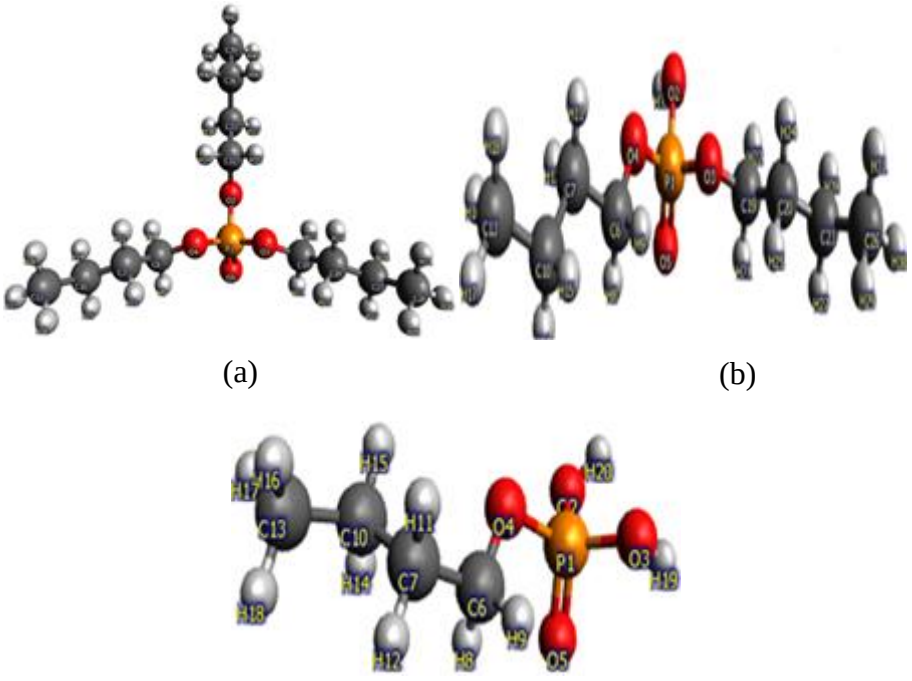

Fig. 1. The optimized molecular structures of (a) TBP, (b) HDBP and (c) H2MBP.

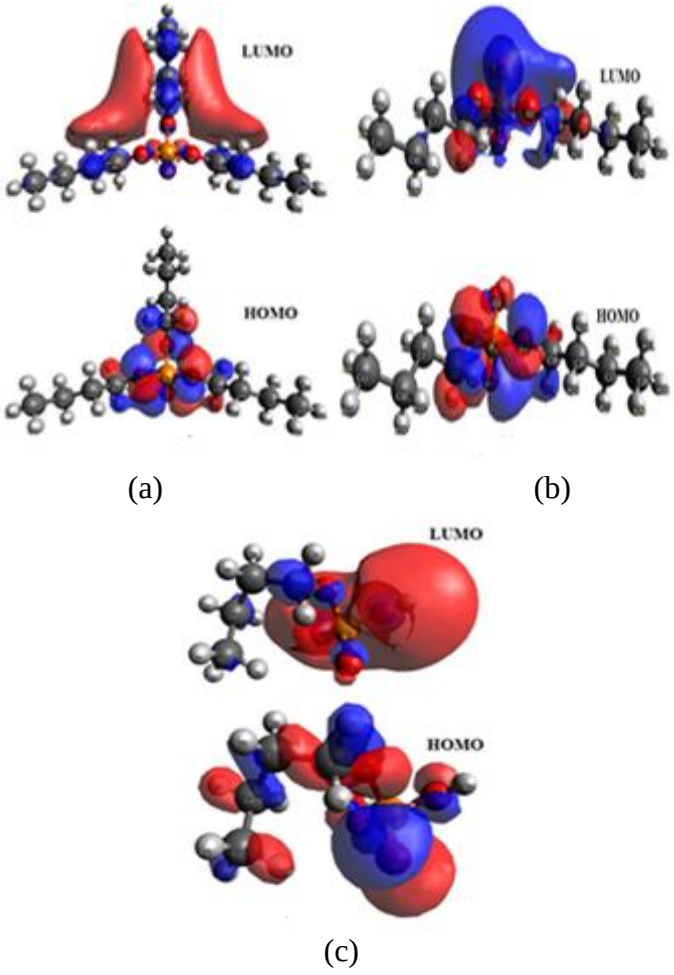

Fig. 2. Frontier orbitals HOMO and LUMO of (a) TBP, (b) HDBP and (c) H2MBP.

Table 1. Total energy Et, dipole moment μ, energy of HOMO and LUMO, Eg (HOMO–LUMO gap) for TBP, HDBP, H_2MBP.

Parameters	TBP	HDBP	H_2MBP
Et (eV)	-30356.787	-26080.039	-21803.0947
HOMO (eV)	-7.791	-7.836	-8.167
LUMO(eV)	0.828	0.691	0.137
ΔEg (eV)	8.619	8.527	8.304
μ (D)	3.176	1.324	3.788

3.2. Dipole moment

The dipole moment of each compound was calculated and is shown in Table 1. The results clearly demonstrate the influence of the hydroxyl groups on the dipole moment. The hydroxyl groups play a major role in increasing the dipole moment. The TBP has the lowest dipole moment as compared with its derivatives, HDBP and H_2MBP, and therefore less stable in polar media.

3.3. Mulliken charge distributions

The computed Mulliken atomic charges are shown in Fig. 3. The variations observed in the carbon atoms involved in the degradation stages (C6, C19 and C32) are simplified and presented in Table 2. The positive charges that appeared on these carbon atoms indicate the polarization of C-O bonds to the phosphorus group and the resultant weakness of these bonds.

When the two hydroxyl groups have been formed (H_2MBP), the carbon (C_6) attached to phosphorus became more stable because the donation of electrons by a hydroxyl group and no further reaction was observed. In contrast, the negative charges on the oxygen (O_2 and O_3) were reduced by the loss of the n-alkyl side chain. This behavior can be attributed to the increment in the ability to donate their lone pairs of electrons.

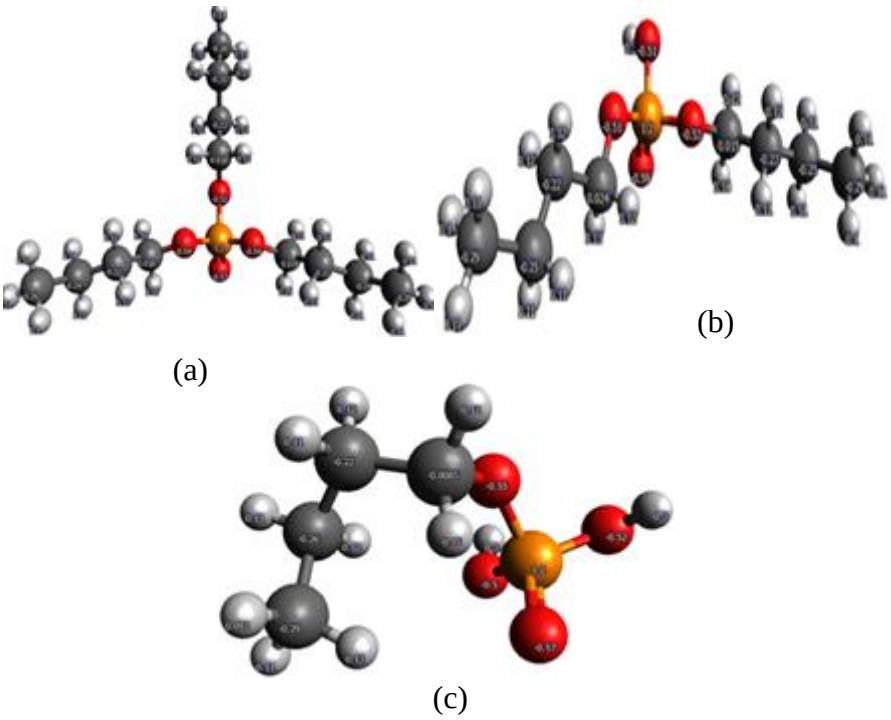

Fig. 3. Mulliken charges distribution indicated on each atom of (a) TBP, (b) HDBP and (c) H2MBP.

Table 2. Mulliken atomic charges of TBP, HDBP and H_2MBP.

Atom	TBP	HDBP	H_2MBP
P	1.3	1.2	1.2
O2	-0.52	-0.51	-0.50
O3	-0.54	-0.53	-0.52
O4	-0.54	-0.51	-0.55
O5	-0.57	-0.59	-0.57
C6	0.018	0.024	-0.0085
C7	-0.22	-0.22	-0.22
C10	-0.24	-0.25	-0.26
C13	-0.29	-0.29	-0.29
C19	0.019	0.015	—
C20	-0.22	-0.23	—
C23	-0.24	-0.25	—
C26	-0.29	-0.29	—
C32	0.018	—	—
C33	-0.23	—	—
C36	-0.25	—	—
C39	-0.28	—	—
H attached to O2	—	0.30	0.30
H attached to O3	—	—	0.30

3.4. Molecular electrostatic potentials (MEP)

The electrostatic potential produced by total charge distribution around a molecule is called molecular electrostatic potential (MEP). MEP illustrates different polarity regions of the molecule that display the electrophilic and nucleophilic reactivity. Color coding is used to represent the different values of the electrostatic potential, positive electrostatic potential regions are represented by blue color, negative the regions are shown in red color, while white represents the region of zero potential. For greater clarity, in Fig. 4, the surfaces of MEP are displayed as viewed from two sides of view. Electronegative regions of the three title molecules are localized on oxygen atoms. An intermediate potential (zero potential) is located around phosphine and carbon atoms and electropositive surfaces are attributed to hydrogen atoms. In HDBP and H_2MBP, the large positive charge of hydrogen atoms attached with oxygen is advantageous for more dense electropositive potential (more blue color) due to the presence of high donated electrons in the hydroxyl groups. In reference to the previous findings, all hydrogen atoms are spots for electrophilic reactivity, while oxygen atoms are their nucleophilic reaction partners.

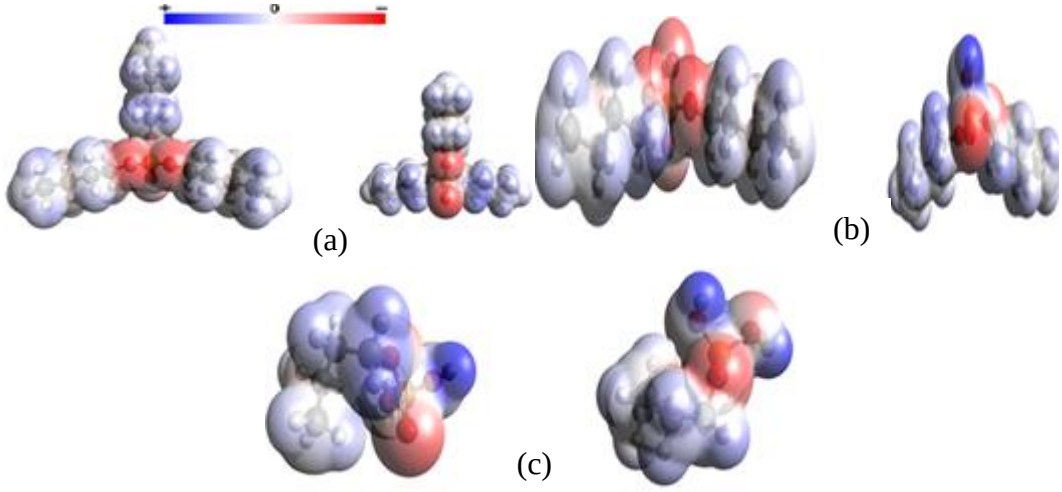

Fig. 4. The molecular electrostatic potential maps around (a) TBP, (b) HDBP and (c) H_2MBP. For clear vision two plots has been taken, forward side (left) and backward (right) for all molecules.

3.5 Fourier transform infrared spectroscopy (FTIR)

FTIR is an important technique for a qualitative analysis of these compounds as illustrated in Fig. 5. The presence of the TBP compound can be easily demonstrated by the absence of the hydroxyl group band, the presence of two bands at 3024 cm^{-1} and 3084 cm^{-1} for C-H stretching, and band at 1297 cm^{-1} for P-O stretching. The P=O bond is shown up as a weak band at 1422 cm^{-1}. Whereas the spectrum of the HDBP compound is very similar to that of the H_2MBP compound. The difference lies in the area of , the fingerprint region. In addition, the transmittance intensity of the hydroxyl group in H_2MBP has increased approximately by one order of magnitude above that of HDBP. Further, the symmetric and asymmetric C-H stretching was clearly evident in TBP and HDBP while the symmetric stretching in H_2MBP was less. It is noteworthy that the transmittance intensity of C-H stretching decreased when the presence of an additional hydroxyl group as in H_2MBP. In contrast, the transmittance intensity of P=O stretching (ranging between 1283 and 1310) was greater in TBP.

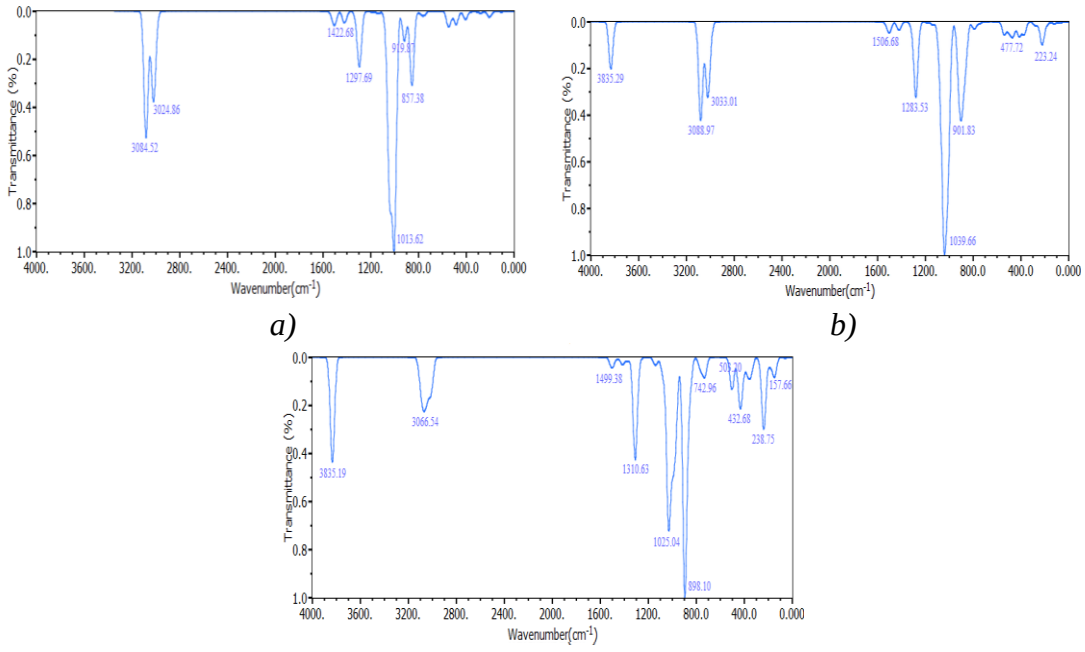

Fig. 5. Fourier transforms infrared spectra (a) TBP, (b) HDBP and (c) H_2MBP.

3.6. Raman spectroscopy

Fig. 6 shows the Raman spectra of TBP, HDBP and H_2MBP. TBP has two distinct bands at 3081 and 3022 cm^{-1}. For HDBP, the band at 3081 shifted to 3089 cm^{-1} while 3022 remained fixed in its place. In contrast, in H_2MBP the positions of the two bands shifted to 3053 and 3032cm^{-1} and the intensity ratio between 3053 and 3032cm^{-1} remained almost unchanged. It is worth mentioning that the TBP qualitatively analyzed by the absence of a hydroxyl group band. Meanwhile, the intensity of the hydroxyl group in H_2MBP increased by two orders of magnitude approximately above that of HDBP.

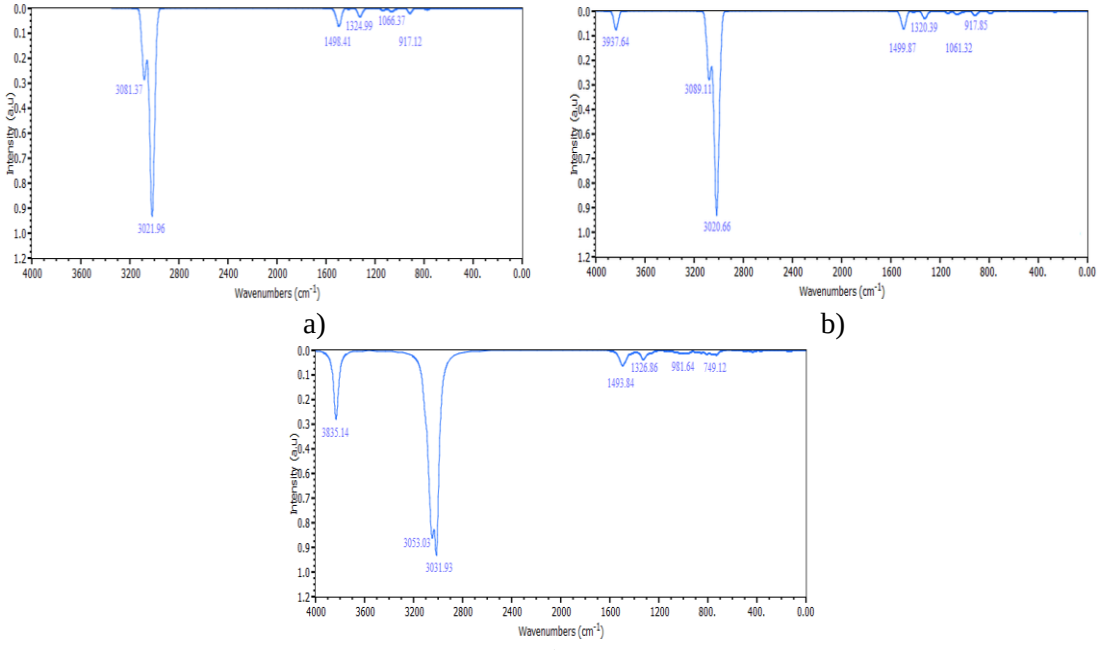

Fig. 6. Raman spectra (a) TBP, (b) HDBP and (c) H_2MBP.

4. Conclusions

To recapitulate, in this work the structural and spectral of TBP, HDBP and H_2MBP were thoroughly studied. The frontier molecular orbitals, HOMO-LUMO transitions, the energy bandgap, dipole moment, electron charges distribution, and Raman and Infrared spectra were computed using DFT. The HOMO-LUMO transitions showed that the energy gap of TBP is greater than the energy band gaps of its depravities.

The dipole moments of the byproducts are higher than the mother compound. The simulated spectra of FTIR and Raman suggested that these can be considered as powerful techniques for qualitative analysis of these compounds. Further, Mulliken charge distributions, molecular orbitals and molecular electrostatic potential (MEP) were significantly affected after the derivatization takes place, particularly at the end side chain of alkyl attached to the phosphorous group.

References

[1] R. Zheng et al., Minerals 8(5), 206 (2018).
[2] S. M. Açıkel, Sakarya University Journal of Science 22(5), 260 (2018).
[3] S.-Y. Lu et al., Environmental science & technology 51(4), 2427 (2017).
[4] J. Kong et al., Journal of pharmaceutical and biomedical analysis 154, 191 (2018).
[5] Z. Dzhivanova et al., Journal of Radioanalytical and Nuclear Chemistry 1 (2019).
[6] R. Ngelale et al., Solvent Extraction and Ion Exchange 37(1), 38 (2019).
[7] H. Kim et al., Industrial & Engineering Chemistry Research 56(12), 3399 (2017).
[8] S. A. Graves et al., Nuclear medicine and biology 64, 1 (2018).
[9] A. G. Baldwin et al., Journal of Molecular Liquids 246, 225 (2017).
[10] L. Zhou et al., Science of The Total Environment 603, 77 (2017).
[11] J. Liu et al., Environmental Pollution 250, 284 (2019).
[12] O. R. da Rocha et al., Brazilian Journal of Chemical Engineering 36(2), 669 (2019).
[13] B. Rowling et al., Journal of environmental radioactivity 178, 377 (2017).
[14] M. Garcia, I. Rodriguez, R. Cela, Journal of chromatography A 1152(1-2), 280 (2007).
[15] B. J. Mincher, G. Modolo, S. P. Mezyk, Solvent Extraction and Ion Exchange 27(1), 1 (2009).
[16] Z. Dzhivanova et al., Progress in Nuclear Energy, 103174 (2019).
[17] A. Dodi, G. Verda, Journal of Chromatography A 920(1-2), 275 (2001).
[18] A. Wright, P. Paviet-Hartmann, Separation Science and Technology 45(12-13), 1753 (2010).
[19] A. Das, P. Sahu, S. M. Ali, Journal of Chemical & Engineering Data 62(8), 2280 (2017).
[20] E. Grabias, M. Majdan, Journal of radioanalytical and nuclear chemistry 313(2), 455 (2017).
[21] K. Jeong, S. M. Woo, S. Bae, Journal of Nuclear Science and Technology 55(4), 424 (2018).
[22] S. Disale et al., Journal of Coordination Chemistry, 1 (2019).
[23] L. Xu et al., Inorganic chemistry 58(7), 4420 (2019).
[24] F. Neese, F., S Interdisciplinary Reviews: Computational Molecular Science 8(1), e1327 (2018).
[25] Munir, T., Kashif, M., Hussain, W., Shahzad, A., Imran, M., Ahmed, A., Amin, N., Ahmed, N., Hussain, A. and Noreen, M., FIRST PRINCIPLES STUDY OF STRUCTURAL AND ELECTRONIC PROPERTIES OF Ti DOPED ZnO. Journal of Ovonic Research, 14(5), (2018).
[26] Ibnaouf, K.H., Hussein, R.K., Elkhair, H.M. and Elzupir, A.O., Experimental and theoretical study of the structure, frontier molecular orbital, tautomerism and spectral analysis of 3-(p-substituted phenyl)-5-phenyl-1H-pyrazole. Journal of Molecular Liquids, 287, 110675. (2019).
[27] Elzupir, A.O., Ali, M.K.M., Hussein, R.K., Ibrahem, M.A., Al-Muhanna, M.K. and Ibnaouf, K.H., 2019. Molecular structure, frontier molecular orbital and spectral analysis of dimethylamino chalcones efficient lasing dyes. Journal of Molecular Structure, 1178, pp.285-289.

[28] M. D. Hanwell et al., Journal of cheminformatics **4**(1), 17 (2012).
[29] A. R. Allouche, Journal of computational chemistry **32**(1), 174 (2011).